Camptothecin improves sorafenib sensitivity by inhibiting Nrf2-ARE pathway in hepatocellular carcinoma

LIWEI SUN[1,2*], HANKANG WANG[1,2*], QIAN LIU[3], FANGUANG MENG[1], JINLIANG ZHANG[1,2], XIAODONG LI[1,2], SHULIN CHANG[1,2], GUIJIE LI[1] and FENG CHEN[1]

[1]Department of Radiology, The First Affiliated Hospital of Shandong First Medical University and Shandong Provincial Qianfoshan Hospital, Shandong Medicine and Health Key Laboratory of Abdominal Medicine Imaging, Jinan, Shandong 250014; [2]Graduate School, Shandong First Medical University and Shandong Academy of Medical Sciences, Jinan, Shandong 250024; [3]Department of Radiology, The Second Affiliated Hospital of Zhejiang University School of Medicine, Hangzhou, Zhejiang 310003, P.R. China

Received October 19, 2022; Accepted January 18, 2023

DOI: 10.3892/or.2023.8492

Abstract. Sorafenib is a targeted drug for hepatocellular carcinoma (HCC), however, its efficacy is limited. Nuclear factor erythroid 2-related factor 2 (Nrf2) contributes to sorafenib resistance. The present study investigated camptothecin (CPT) as a Nrf2 inhibitor to sensitize HCC to sorafenib. The effect of CPT on sorafenib sensitivity in HCC was assessed *in vivo* using H22 mice model (n=32) and VX2 rabbit models (n=32), which were sorted into four treatment groups. The expression levels of Nrf2, its downstream genes, including heme oxygenases-1 (HO-1) and NAD(P)H quinone oxidoreductase 1 (NQO1), and the epithelial-mesenchymal transition markers Snail and N-cadherin in tumors were determined using immunohistochemical staining and western blotting. Magnetic resonance imaging was used to monitor changes in tumor microcirculation and activity before and after treatment. Mouse body weights, liver and kidney function were monitored to evaluate the safety of combined therapy. The results revealed that the mean tumor size of the combined group was significantly smaller than that of sorafenib group for both models. The expression levels of Nrf2, heme oxygenase-1, NAD(P)H quinone oxidoreductase 1, Snail, and N-cadherin in the sorafenib group were significantly higher than control group (P<0.05). However, the expression levels of these genes were decreased in the combined group (P<0.05). Microcirculation perfusion and tumor activity in the combined group were also lower than sorafenib group. There were no significant differences in mouse body weight or liver and kidney function among the four groups. In summary, CPT is a Nrf2 inhibitor that could enhance the efficacy of sorafenib against HCC.

Correspondence to: Dr Feng Chen or Dr Guijie Li, Department of Radiology, The First Affiliated Hospital of Shandong First Medical University and Shandong Provincial Qianfoshan Hospital, Shandong Medicine and Health Key Laboratory of Abdominal Medicine Imaging, 16766 Jingshi Road, Lixia, Jinan, Shandong 250014, P.R. China
E-mail: fengxiao6556@126.com
E-mail: sdulgj@163.com

*Contributed equally

Key words: hepatocellular carcinoma, camptothecin, sorafenib, Nrf2, chemoresistance

Introduction

Primary liver cancer is the sixth most common cancer (4.7%) and the third most common cause of cancer-related death (8.3%) in 2020 and hepatocellular carcinoma (HCC) comprises 75-85% of cases (1). Due to the occult onset and rapid progression of HCC, patients are often diagnosed at an advanced stage, which severely limits treatment options (2). Potentially curative therapies (e.g. transplantation, resection, or ablation) are only suitable for less than 30% of patients (3). Sorafenib was the only approved tyrosine kinase inhibitor for patients with unresectable HCC from 2007 to 2018. This drug blocks the proliferation of tumor cells and inhibits angiogenesis by suppressing the RAF/MEK/ERK pathway and inhibiting vascular endothelial growth factor receptor 2/3 (VEGFR-2/3) and platelet-derived growth factor receptor (2-4). Sorafenib can prolong survival by three to five months according to the SHARP phase III clinical trial (2,5,6,7). Nevertheless, this effect is limited due to acquired drug resistance (5,8).

A hypoxic tumor microenvironment, the epithelial-mesenchymal transition (EMT), epigenetic regulation, and ferroptosis are mechanisms of sorafenib resistance in HCC inextricably linked to nuclear factor erythroid 2-related factor 2 (Nrf2) (5). According to a recent study, sorafenib significantly induced Nrf2 protein expression, but not its mRNA expression (6). At present, the most studied mechanism is ferroptosis. Ferroptosis involves generation of iron-dependent accumulation of lipid reactive oxygen species (ROS), which can be regulated by cystine glutamate reverse transporter (systemx_{c^-}) and glutathione peroxidase 4 (GPX4) (6). Systemx_{c^-} transports the extracellular cystine to the inside of the cell, and

then converts it into cysteine to synthesize the antioxidant glutathione (GSH). Under normal conditions, GPX4 prevents ferroptosis by inhibiting the accumulation of lipid peroxides in cells. When GPX4 is inhibited, it can lead to the accumulation of ROS in cells, thus inducing ferroptosis. GSH is an indispensable cofactor in its activation process. Sorafenib inhibits systemx_{c^-}, which leads to the accumulation of ROS in the cell, thus triggering ferroptosis (9). In previous studies, the expression of Nrf2 increased in response to cell oxidative stress and the accumulation of ROS (10), which reduced tumor cells ferroptosis and caused sorafenib resistance. As certain ABC transporters are downstream proteins, the absence of Nrf2 also increases sorafenib sensitivity (8,10-13). Cancer stem cells, which mediate the formation and growth of tumor tissue and the intrinsic resistance to chemotherapy drugs, highly express Nrf2 (8,10,14-16). Nrf2 also upregulates the expression of Bcl-2 and Bcl-Xl, which encode two antiapoptotic factors (11-13,17). These studies also highlight the importance of Nrf2 in sorafenib resistance.

Nrf2 is encoded by the erythroid 2-like 2 (NFE2L2) gene (18-23). Under normal circumstances, Kelch-like ECH-associated protein (Keap1) binds Nrf2, leading to its proteasomal degradation in the cytoplasm (6,18-22,24). During oxidative stress, electrophiles and ROS react with Keap1, dissociating it from Nrf2, which translocates to the nucleus and activates antioxidant response elements (ARE). ARE-mediated cytoprotective proteins include antioxidant enzymes, stress response proteins, metal-binding proteins, drug-metabolizing enzymes and drug transporters (22). Carcinogenesis is also a newly defined function of Nrf2 (18,19,22). Nrf2 activation can protect cells against chemicals that cause cancer for a limited period; however, constant hyperactivation of Nrf2 is frequently observed in HCC and is related to poor outcome (25-27).

Camptothecin (CPT) is a natural alkaloid that is an effective antitumor agent. It binds to DNA topoisomerase I to suppress DNA replication (10,26,28). Previous studies by the authors confirmed that CPT is an Nrf2 inhibitor that is effective at lower concentrations, which reduces drug toxicity (10,26). CPT can be combined with anticancer drugs that increase the level of Nrf2 to treat HCC (10). Based on the aforementioned studies, it was hypothesized that CPT could improve the sensitivity of HCC to sorafenib by inhibiting the NRF2-ARE pathway. In the present study, two liver tumor models (H22 and VX2) were generated to test this hypothesis by comparing the tumor response and Nrf2 protein levels of sorafenib monotherapy and the combined treatment of CPT and sorafenib.

Materials and methods

H22 HCC model. All animal experiments were performed according to the ARRIVE guidelines approved (approval no. S0007) by the Animal Care and Use Committee of the First Hospital of Shandong First Medical University (Jinan, China). Male BALB/c mice (4-6 weeks old, 20-23 g) were divided into two batches (n=20/batch), maintained under standard animal housing conditions with room temperature, adequate air, a 12/12-h light/dark cycle and were allowed access *ad libitum* to sterilized water and chow diet. H22 cells ($1x10^6$/200 μl normal saline) were inoculated subcutaneously into the mice. When the tumors reached the size of a soybean grain, the mice underwent magnetic resonance imaging (MRI) to measure the maximum cross sections, activity, and microcirculation perfusion of the tumors. A total of 16 mice with similar tumor sizes were selected from each batch and divided into four treatment groups: control (CTR) group (normal saline), CPT group (1 mg/kg CPT), sorafenib (SOR) group (50 mg/kg sorafenib), and combined (COM) group (1 mg/kg CPT + 50 mg/kg sorafenib). CPT was administered by intraperitoneal injection every three days, and sorafenib was administered daily by gavage. The first administration of drugs was conducted on the second day after MRI. A second MRI was performed 18 days later. A total of 40 mice model were established in the experiment, of which 32 were qualified for inclusion, 8 were not included in the group and euthanized by injection of pentobarbital sodium. A total of 32 mice survived to the end of the experiment in a favorable state and were euthanized by injection of pentobarbital sodium. The method of euthanasia of mice was 2% pentobarbital sodium slowly intraperitoneally injected to death. Finally, the tumors were isolated after euthanasia of mice, and the mice were weighed following tumor removal. The tumor volume, MRI data and body weights were analyzed to determine the tumor response and detect drug toxicity. The analysis was performed using GraphPad Prism software (version 8; GraphPad Software, Inc.).

VX2 liver tumor model. To generate tumor pieces for implantation into experimental rabbits, VX2 tumor pieces were implanted intramuscularly into the hind limbs of young rabbits. After two weeks, the tumors were resected and milled. Using ultrasound guidance, 1 mm^3 VX2 tumor tissue was implanted in the left lobe of the livers of forty male New Zealand white rabbits (3.0-3.5 kg) at a depth of 1.5 cm. After 14 days, MRI was performed to measure tumor activity and to select 32 rabbits with similar tumor sizes. The rabbits were randomly divided into four groups (n=8): CTR group (normal saline), CPT group (3 mg/kg CPT), SOR group [transcatheter arterial embolization (TAE), 3 mg/kg sorafenib], and COM groups (1 mg/kg CPT + 3 mg/kg sorafenib, TAE). TAE was performed under digital subtraction angiography guidance. Lipiodol (0.1-0.5 ml) and sorafenib were injected into the tumor-feeding arteries. CPT was administered by intraperitoneal injection every three days. MRI was performed again nine days after the first treatment. A total of 36 rabbit models were established in the experiment, of which 32 were qualified for inclusion, 4 were not included in the group and euthanized by injection of pentobarbital sodium. A total of 36 rabbits survived to the end of the experiment in a favorable state and were euthanized by injection of pentobarbital sodium. The method of euthanasia of rabbits was 3% pentobarbital sodium slowly intraperitoneally injected to death. Next, the tumors were resected after euthanasia of rabbits, and tumor-free rabbits were weighed. The MRI data, and the weight of tumor-free rabbits were analyzed by GraphPad Prism software and used to represent the tumor response and detect the drug toxicity.

Rabbits and mice were provided by Beijing Weitong Lihua Company. HCC and VX2 tumors are provided by the laboratory of Qianfo Mountain Hospital. All animal welfare was taken into consideration, including efforts to minimize suffering and distress, use of analgesics or anesthetics, or

special housing conditions. The duration of the experiment of the H22 mice model was 32 days. The duration of the experiment of the VX2 rabbit models was 37 days. When the goal of the experiment was completed, the animals were treated in a scientific and humane way so as to minimize the panic and pain of the animals and being subjected to euthanasia gently and quickly. Through the observation of respiratory and heartbeat cessation, pupil, nerve reflex and other indicators, a comprehensive judgment on death was determined, confirming that the experimental animal had succumbed.

Magnetic resonance imaging

Mice. MRI included T2-weighted imaging (T2WI), and intravoxel incoherent motion (IVIM) (GE, 3.0T MR scanner, mouse coil). The T2WI sequence was performed using a repetition time (TR) of 2,200 ms, echo time (TE) of 102.0 ms, slice thickness of 1.5 mm, and a NEX of 2.0. The IVIM sequence was performed using a TR of 2,000 ms, a minimum TE, a slice thickness of 1.0 mm, and b=0, 50, 100, 150, 200, 400, 600, 800, 1,000 and 1,200 s/mm^2. All images were sent to a workstation for post-processing. The largest cross-sections of the tumors were marked and used to assess tumor growth, and the Standard apparent diffusion coefficient (Standard ADC, representing an average diffusion value), diffusion coefficient (D, reflecting the diffusion of pure water molecules), pseudo-diffusion coefficient (D*, reflecting the microcirculation perfusion), and perfusion fraction (f, defined as the ratio between the perfusion of local microcirculation and diffusion in overall) in these areas were also determined. Changes in the ADC (ΔADC), D (ΔD), D* (ΔD*), and f (Δf) were calculated by subtracting the preoperative values from the postoperative values and used to assess the changes of tumor activity and microcirculation perfusion after treatment.

Rabbits. MRI included T2WI and diffusion-weighted imaging (DWI) scans (GE, 3.0T MR scanner, Knee coil). The T2 sequence consisted of a TR of 5,200 ms, TE of 88.7 ms, slice thickness of 2 mm and a NEX of 2.0. The DWI sequence was performed using a TR of 4,500 ms, a TE of 81.6 ms, a slice thickness of 2 mm, a NEX of 2.0, and b=0, 800 s/mm^2. Post-processing was performed after the images were transmitted to the workstation. The largest cross-sections of the tumors were marked, and the ADC values (representing an average diffusion value) within the areas were measured. The changes in ADC (ΔADC, postoperative ADC-preoperative ADC) were calculated to assess the changes of tumor activity after treatment.

Haematoxylin and eosin (H&E) staining. The lungs, livers and kidneys from H22 and VX2 tumor-bearing animals were fixed in polyformaldehyde (4%) and embedded in paraffin wax at room temperature. Sections of 4-μm thickness were cut, mounted on charged glass slides and then stained with haematoxylin and eosin at room temperature. Briefly, hematoxylin was added to the sections for 10 min. Then, 1% acid ethanol reagent was used to differentiate for 1 min. Then, the blue returning liquid promoted the nucleus to return blue, and then the eosin solution was incubated with sections for 3 min. Finally, the sections were dehydrated and fixed with neutral balsam. The image was collected under the optical microscope.

Immunohistochemical (IHC) staining. The reagents and steps for tissue fixation, paraffin embedding and sectioning were as H&E staining. Paraffin sections (4-μm) of H22 and VX2 tumors were deparaffinized with xylene and rehydrated with descending ethanol series. Sections were blocked with BSA at 37˚C for 30 min and covered with antibody against Nrf2 (1:2,000; cat. no. GB113808), VEGFA (1:500; cat. no. GB14165), hypoxia-inducible factor-1α (HIF-1α) (1:1,000; cat. no. APR07746G), N-cadherin (1:1,500; cat. no. GB111273) and Snail (1:800; cat. no. GB11260) at 4˚C, overnight. Antibodies against Nrf2, VEGFA, N-cadherin, Snail were obtained from Wuhan Servicebio Technology Co., Ltd. Antibodies against HIF-1α were obtained from Santa Cruz Biotechnology, Inc. Then, the sections were incubated with HRP-labeled Goat Anti-Rabbit IgG solution (cat. no. G1213-100UL) and HRP-labeled Goat Anti-Mouse IgG solution (cat. no. G1214-100UL; both from Wuhan Servicebio Technology Co., Ltd.) at dilutions of 1:200 at 37˚C for 30 min, and then were added with DAB substrate. Nuclei were counterstained with haematoxylin. The image was collected under the optical microscope. Staining was visualized using Image-Pro Plus 6 software (Media Cybernetics, Inc.), and the integrated optical density/Area values were used to determine protein expression levels in the tumors.

Western blotting (WB). The H22 and VX2 tumors were smashed in the RIPA (Wuhan Servicebio Technology Co., Ltd.) buffer with 1 mM PMSF on ice and then centrifuged as previously described (26). Bicinchoninic acid (BCA) was used to determinate protein concentration. Protein samples (15 μg samples per lane) were loaded into 30% SDS-PAGE gels and transferred to PVDF membranes. The membranes were blocked with 3% BSA at room temperature for 1 h and incubated at 4˚C overnight with the following primary antibodies (obtained from Wuhan Servicebio Technology Co., Ltd.): Nrf2 (1:1,000), heme oxygenase-1 (HO-1) (1:1,000; cat. no. GB12104), NAD(P)H quinone oxidoreductase 1 (NQO1) (1:500; cat. no. GB11282), N-cadherin (1:500) and Snail (1:800). Then, the membranes were incubated with HRP-labeled Goat Anti-Rabbit IgG solution and HRP-labeled Goat Anti-Mouse IgG solution at dilutions of 1:5,000 at room temperature for 1 h. Finally, membranes were covered with enhanced chemiluminescent (ECL) substrate and scanned. ECL substrate was obtained from Merck Millipore. Quantification of the results normalized to β-actin was conducted using Image J software (version 1.8.0.345; National Institutes of Health).

Serum biochemistry. The health and behavior of H22 mice model were monitored every day after H22 cells were inoculated subcutaneously into the mice. The health and behavior of VX2 rabbit models were monitored in three days before operation and in day 1, 4, 7, 10, 13, 14 after operation. Blood was collected via the retro-orbital sinus and was centrifuged at 4˚C, 1,000 x g for 5 min. Aspartate aminotransferase, alanine aminotransferase, blood urea nitrogen, creatinine and total bilirubin levels were measured using an automatic biochemical analyzer.

Statistical analysis. GraphPad Prism software was used to analyze all experiments. Data are presented as the mean ± SD.

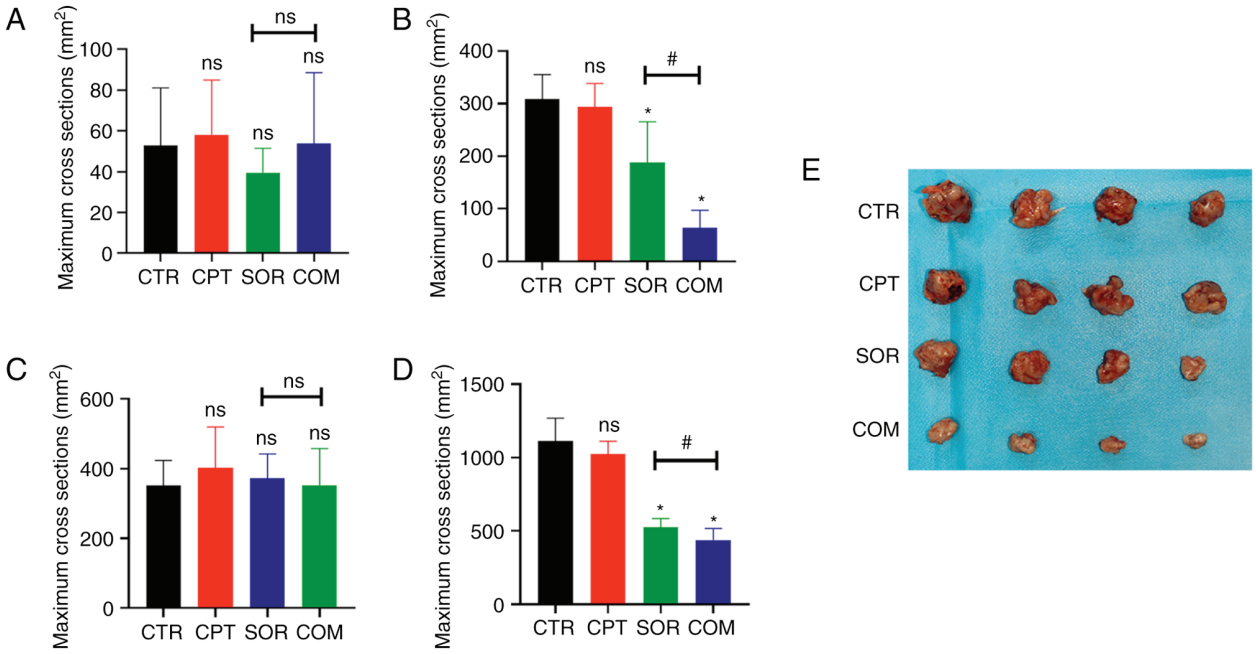

Figure 1. CPT combined with sorafenib therapy inhibits tumor growth in H22 and VX2 models. (A and B) The maximum cross sections measured by MRI of H22 models (A) before and (B) after treatment in CTR, CPT, SOR and COM groups, 8 samples per group. (C and D) The maximum cross sections measured by MRI of VX2 models (C) before and after (D) treatment in the four groups, 8 samples per group. (E) Tumor volume of H22 models. *P<0.05 and #P<0.05. CPT, camptothecin; MRI, magnetic resonance imaging; CTR, control; SOR, sorafenib; COM combined; ns, no statistical significance.

Comparisons between groups were performed using one-way ANOVA with Tukey's multiple comparison test as post hoc. P<0.05 was considered to indicate a statistically significant difference.

Results

CPT reverses sorafenib resistance by inhibiting Nrf2-ARE activation. The effects of sorafenib alone or in combination with CPT are presented in Fig. 1. According to the T2WI images, the mean maximum H22 tumor cross sections in the CTR, CPT, SOR, and COM groups before treatment were 52.88±26.45, 58.13±25.13, 39.50±11.8 and 53.75±32.60 mm^2, respectively (P≥0.05) (Fig. 1A). After treatment, the maximum cross sections were 308.5±43.98 mm^2 (CTR), 294±41.64 mm^2 (CPT), 187.75±73.03 (SOR) and 63.75±31.18 mm^2 (COM). There was no significant difference between the mean maximum cross sections of the CTR and CPT groups (P≥0.05). By contrast, the differences between the CTR and SOR groups and the SOR and COM groups were statistically significant (P<0.05) (Fig. 1B). For the VX2 liver tumor model, the mean maximum tumor cross sections before treatment were 352.38±75.67 mm^2 (CTR), 401.88±117.80 mm^2 (CPT), 372.88±69.39 mm^2 (SOR) and 352.75±104.81 mm^2 (COM) (P≥0.05) (Fig. 1C). After treatment, the mean maximum VX2 cross sections were 1,112.13±145.35 mm^2 (CTR), 1,022.38±82.03 mm^2 (CPT), 524.13±56.55 mm^2 (SOR) and 438.50±72.97 mm^2 (COM). The differences of the mean maximum cross sections of the VX2 tumors in the CTR and SOR groups and the SOR and COM groups reached statistical significance (P<0.05) (Fig. 1D). The size of tumors of H22 models is presented in Fig. 1E.

There was no significant difference in the Nrf2 levels in H22 tumors from mice treated with CTR or CPT (P≥0.05). IHC staining showed that the Nrf2 protein was slightly reduced in the CPT group (Fig. 2A and B), but WB showed an increase (Fig. 2C and D). However, sorafenib treatment significantly increased Nrf2 levels compared with the CTR group. This effect was significantly reduced by CPT (COM group) (P<0.05). IHC and WB generated similar results (Fig. 2A-D). In the VX2 liver model, CPT monotherapy caused a slight reduction in the Nrf2 levels in the tumors compared with the CTR group (P<0.05). Similar to the H22 model, sorafenib alone induced Nrf2 protein expression, which was abrogated by combining with CPT (Fig. 2E-H). Furthermore, WB revealed that proteins downstream of Nrf2 (HO-1 and NQO1) changed in a similar manner (Fig. 3).

CPT reverses sorafenib resistance by inhibiting EMT. H&E staining of mouse tissues confirmed there were no obvious metastatic lesions in the lung, liver, or kidney. By contrast, there were obvious metastatic lesions in the lungs of VX2 tumor-bearing animals. The most metastatic lesions were observed in the SOR group, followed by the CTR and CPT groups. The least number of metastases were found in the lungs collected from rabbits in the COM group (Fig. 4A). Therefore, the EMT indexes of the VX2 tumors were examined. Based on IHC and WB, the EMT indexes (Snail and N-cadherin) were lower in the COM group than in the SOR group; these indexes in the SOR group were significantly higher than in the CTR group (P<0.05) (Fig. 4B-I).

CPT combined with sorafenib inhibits angiogenesis. For the VX2 model, the expression levels of HIF-1α and VEGFA in the SOR group were higher than in the CTR and COM groups (P<0.05) (Fig. 5A-D). Moreover, the VEGFA levels in the H22 tumors harvested from mice in the COM group

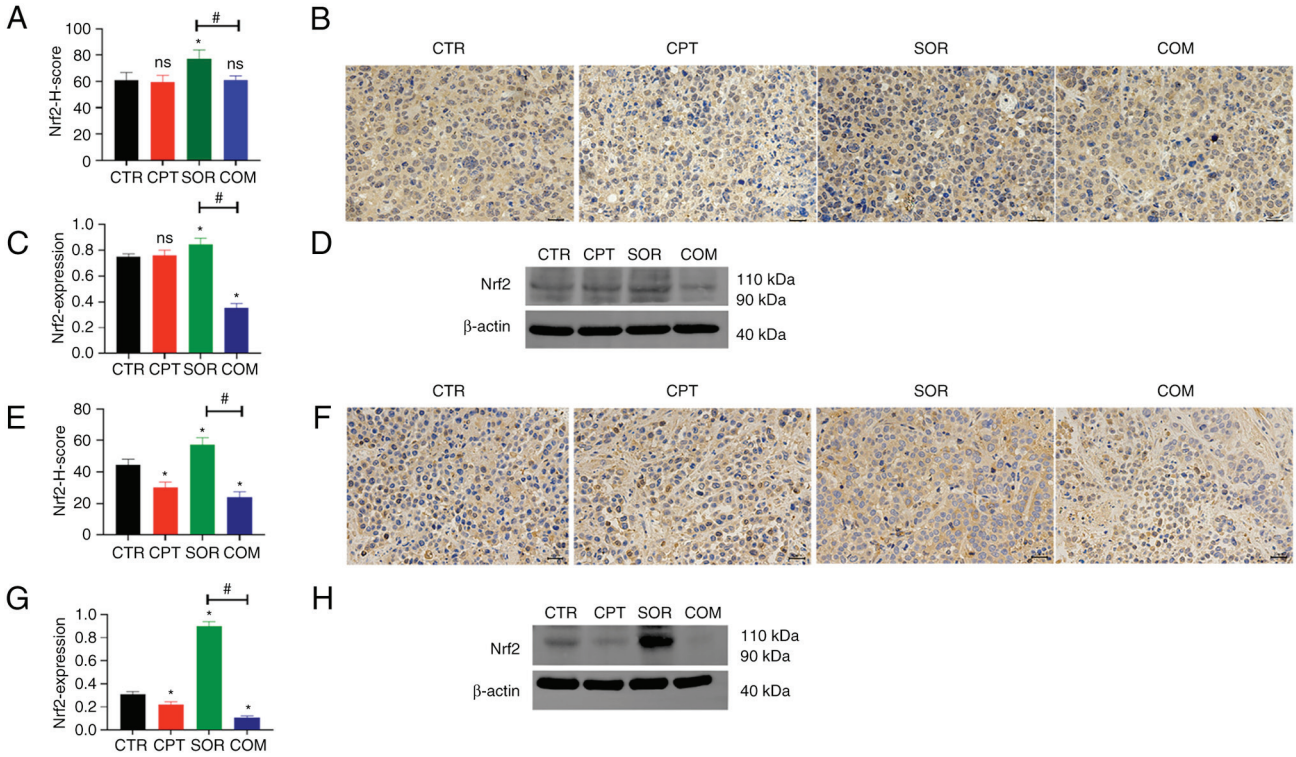

Figure 2. CPT reverses sorafenib resistance by inhibiting Nrf2 activation. (A-D) The Nrf2 expression was determined by (A and B) IHC staining and (C and D) WB in H22 models. The Nrf2 expression was determined by (E and F) IHC and (G and H) WB in VX2 models. Magnification, x400; scale bars, 20 μm. β-actin was the internal control of WB. Panels A, C, E and G demonstrate the statistical analysis for IHC staining and WB (8 samples in each group). *P<0.05 and #P<0.05. CPT, camptothecin; Nrf2, nuclear factor erythroid 2-related factor 2; IHC, immunohistochemical; WB, western blotting; ns, no statistical significance.

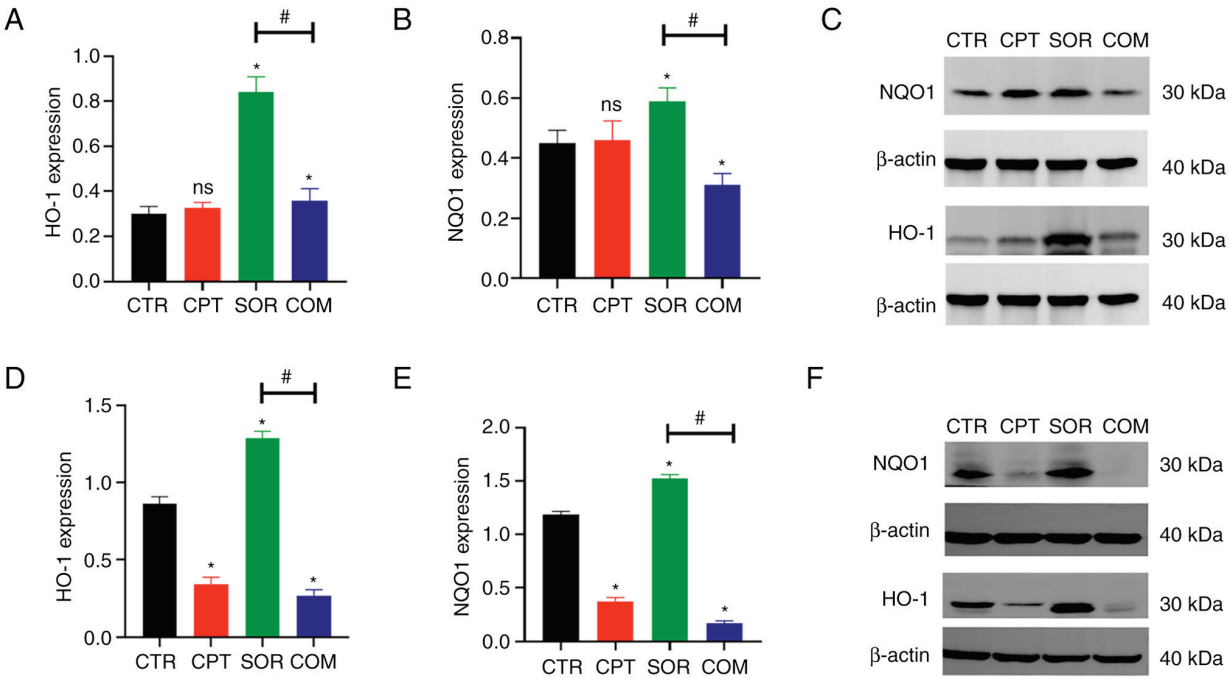

Figure 3. Expression of HO-1 and NQO1 is inhibited after the combined therapy of sorafenib and CPT in H22 and VX2 models. (A-C) The expression of HO-1 and NQO1 was determined by WB in H22 models. (D-F) The expression of HO-1 and NQO1 was determined by WB in VX2 models. β-actin was the internal control of WB. Panels A, B, D and E demonstrate the statistical analysis for WB (8 samples in each group). *P<0.05 and #P<0.05. HO-1, heme oxygenase-1; NQO1, NAD(P)H quinone oxidoreductase 1; CPT, camptothecin; WB, western blotting; ns, no statistical significance.

were significantly lower than in the SOR group (P<0.05) (Fig. 5E and F). MRI analysis of H22 tumors before and after treatment revealed ΔD^* values of -86.25±334.41 (x10^{-5} mm^2/s) for the CTR group, -272.5±218.29 (x10^{-5} mm^2/s) for the CPT

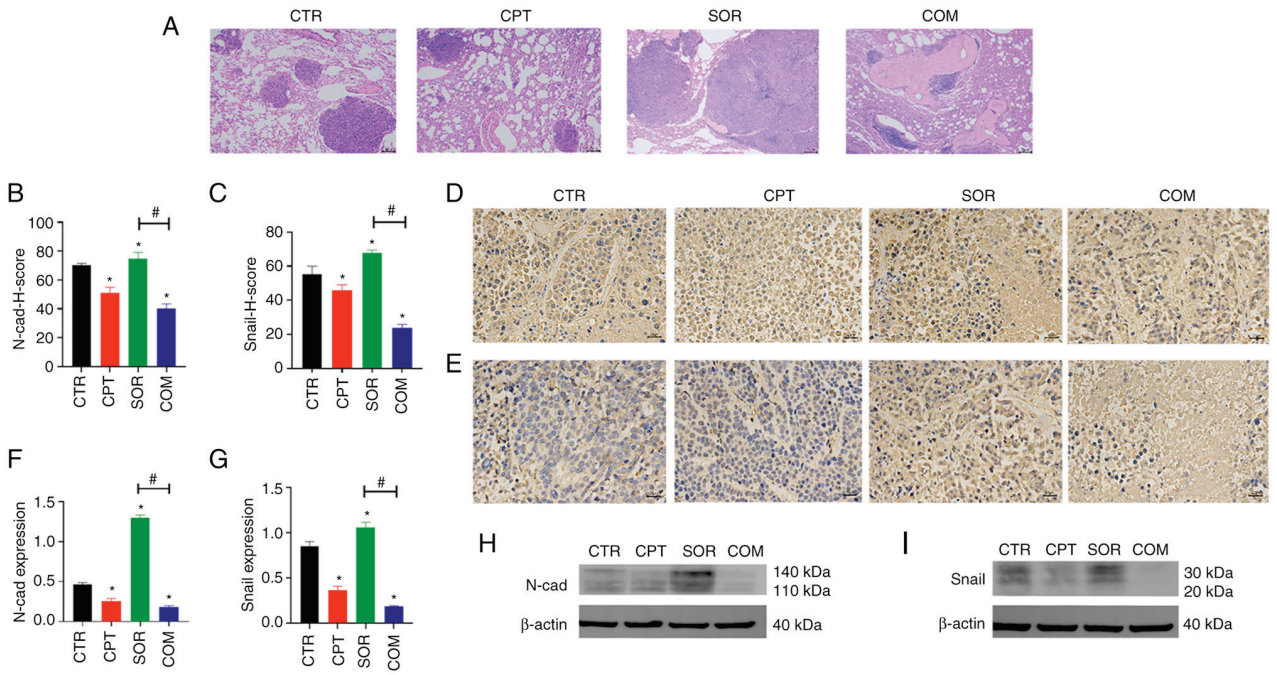

Figure 4. CPT reverses sorafenib resistance by inhibiting the process of EMT. (A) Pulmonary metastases observed by H&E staining in VX2 models. Magnification, x40; scale bars, 2 μm. (B-E) The expression of EMT indexes including N-cad and Snail was determined by IHC staining in VX2 models. Magnification, x400; scale bars, 20 μm. (F-I) The expression of N-cad and Snail determined by WB in VX2 models; β-actin was the internal control. Panels B, C, F and G demonstrate the statistical analysis for IHC staining and WB (8 samples in each group). *P<0.05 and $^{\#}$P<0.05. CPT, camptothecin; EMT, epithelial-mesenchymal transition; H&E, haematoxylin and eosin; N-cad, N-cadherin; IHC, immunohistochemical; WB, western blotting; ns, no statistical significance.

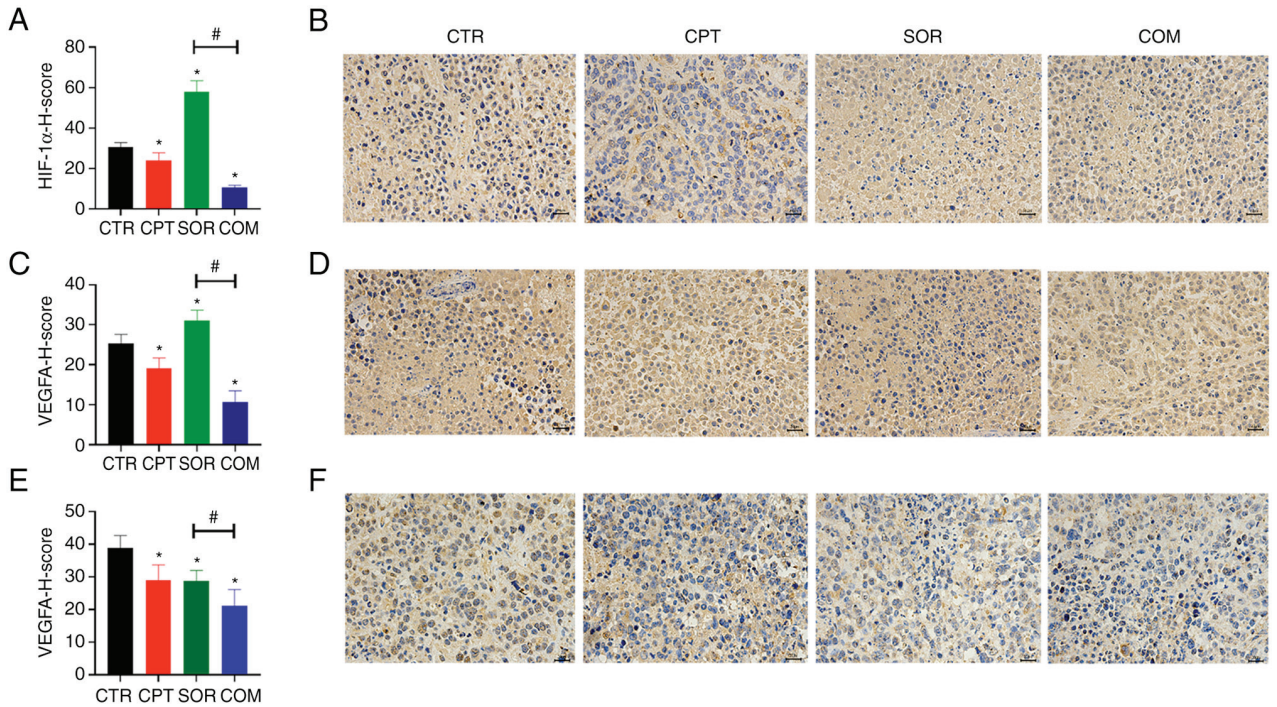

Figure 5. CPT combined with sorafenib inhibits angiogenesis. (A-D) The expression of (A and B) HIF-1α and (C and D) VEGFA was determined by IHC staining in VX2 models. (E and F) The expression of VEGFA was determined by IHC staining in H22 models. Magnification, x400; scale bars, 20 μm. Panels A, C and E demonstrate the statistical analysis for IHC staining (8 samples in each group). *P<0.05 and $^{\#}$P<0.05. CPT, camptothecin; HIF-1α, hypoxia inducible factor-1α; VEGFA, vascular endothelial growth factor receptor A; IHC immunohistochemical; ns, no statistical significance.

group, -240.25±274.89 (x10^{-5} mm^2/s) for the SOR group, and -381.25±206.22 (x10^{-5} mm^2/s) for the COM group. The ΔD^* of the SOR group was slightly lower than that of the CTR group (P≥0.05) and slightly higher than that of the COM group (P≥0.05) (Fig. 6A and B). The Δf values were 0.07±0.26 (CTR), 0.14±0.09 (CPT), -0.01±0.18 (SOR) and -0.18±0.14

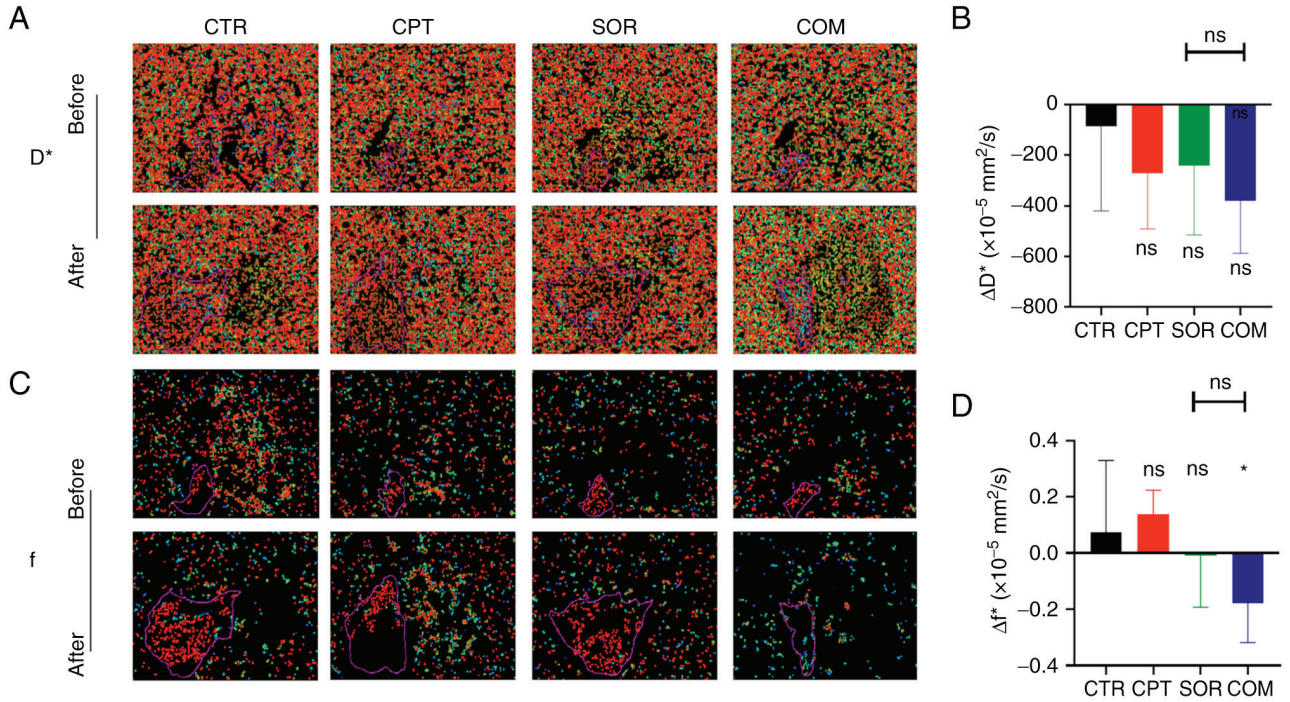

Figure 6. CPT combined with sorafenib decreases microcirculation perfusion. (A) D^* values of CTR, CPT, SOR and COM groups in H22 models before and after treatment. (B) ΔD^* value was calculated in four groups. (C) f values of four groups in H22 models before and after treatment. (D) Δf value was calculated in four groups. The MRI images in panels A and C were enlarged according to the same scale. *P<0.05. CPT, camptothecin; D^*, pseudo-diffusion coefficient; CTR, control; SOR, sorafenib; COM, combined; ΔD^*, postoperative D^* - preoperative D^*; f, perfusion fraction; Δf, postoperative f - preoperative f; ns, no statistical significance.

(COM). The Δf of the SOR group was slightly lower than that of the CTR group (P≥0.05) and slightly higher than that of the COM group (P≥0.05) (Fig. 6C and D).

CPT combined with sorafenib reduces tumor activity. The ΔStandard ADC for H22 tumors was -17.45±36.38 (x10^{-5} mm^2/s) for the CTR group, -29.87±31.05 (x10^{-5} mm^2/s) for the CPT group, 5.76±52.38 (x10^{-5} mm^2/s) for the SOR group and 76.51±98.96 (x10^{-5} mm^2/s) for the COM group. Moreover, the Δ Standard ADC for the SOR group was slightly higher than that of the CTR group (P≥0.05) and slightly lower than that of the COM group (P≥0.05) (Fig. 7A and B). The ΔD was -55.75±42.34 (x10^{-5} mm^2/s) for the CTR group, -39.62±46.48 (x10^{-5} mm^2/s) for the CPT group, -55.75±73.43 (x10^{-5} mm^2/s) for the SOR group and 47.25±36.41 (x10^{-5} mm^2/s) for the COM group. The ΔD of the SOR group was slightly lower than that of the COM group (P≥0.05) (Fig. 7C and D). In the VX2 model, ΔADC showed statistically significant differences between the SOR and CTR groups and the COM and SOR groups (P<0.05) (Fig. 7E and F).

The safety and tolerability of the CPT and sorafenib combination. After treatment and tumor resection, there were no differences in the weights of the mice and rabbits among the four treatment groups. The mouse body weights were 20.25±1.79 g (CTR), 18.75±0.83 g (CPT), 18.88±1.05 g (SOR) and 19.25±1.30 g (COM) (P≥0.05) (Fig. S1A), and the rabbit body weights of the four groups were 3.33±0.09 kg (CTR), 3.29±0.13 kg (CPT), 3.36±0.11 kg (SOR) and 3.33±0.12 kg (COM) (P≥0.05) (Fig. S1B). Serum analysis for the mice revealed that none of the treatments affected liver or kidney function (Fig. S1C-G). There was also no obvious damage in the liver or kidney tissue by H&E staining.

Discussion

Sorafenib improves the survival of patients with advanced HCC. Nevertheless, only ~30% of patients with HCC benefit from sorafenib and usually acquire drug resistance within six months (29). Sorafenib resistance contributes to proliferation, migration and invasion (8). A previous study confirmed that sorafenib-resistant cells had lower proliferation, migration and invasion rates after Nrf2 knockdown (8). Keap1, a redox sensor protein negatively regulating Nrf2, also enhances sorafenib sensitivity in HCC (30). Therefore, the inhibition of Nrf2 in tumors is vital to reversing sorafenib resistance. Brusatol, retinoic acid receptor α agonists, luteolin, and trigonelline are known Nrf2 inhibitors (31-34). In a previous study by the authors (10), CPT was also identified as an effective Nrf2 inhibitor among thousands of clinical drugs.

As an Nrf2 inhibitor, it was hypothesized that CPT could enhance the efficacy of sorafenib. Thus, this hypothesis was examined using two liver cancer models: the H22 murine HCC model and the VX2 orthotopic rabbit liver tumor model. The results of the present study indicated that the CPT-sorafenib combination therapy inhibited tumor growth in the two models. Indeed, the tumors in the COM group were significantly smaller than that in the SOR group. Although the size of the tumors was decreased in the CPT group of the H22-bearing mice compared with the CTR group, the changes were not statistically significant. These data indicated that in this model, CPT was acting as a sensitizer of sorafenib rather

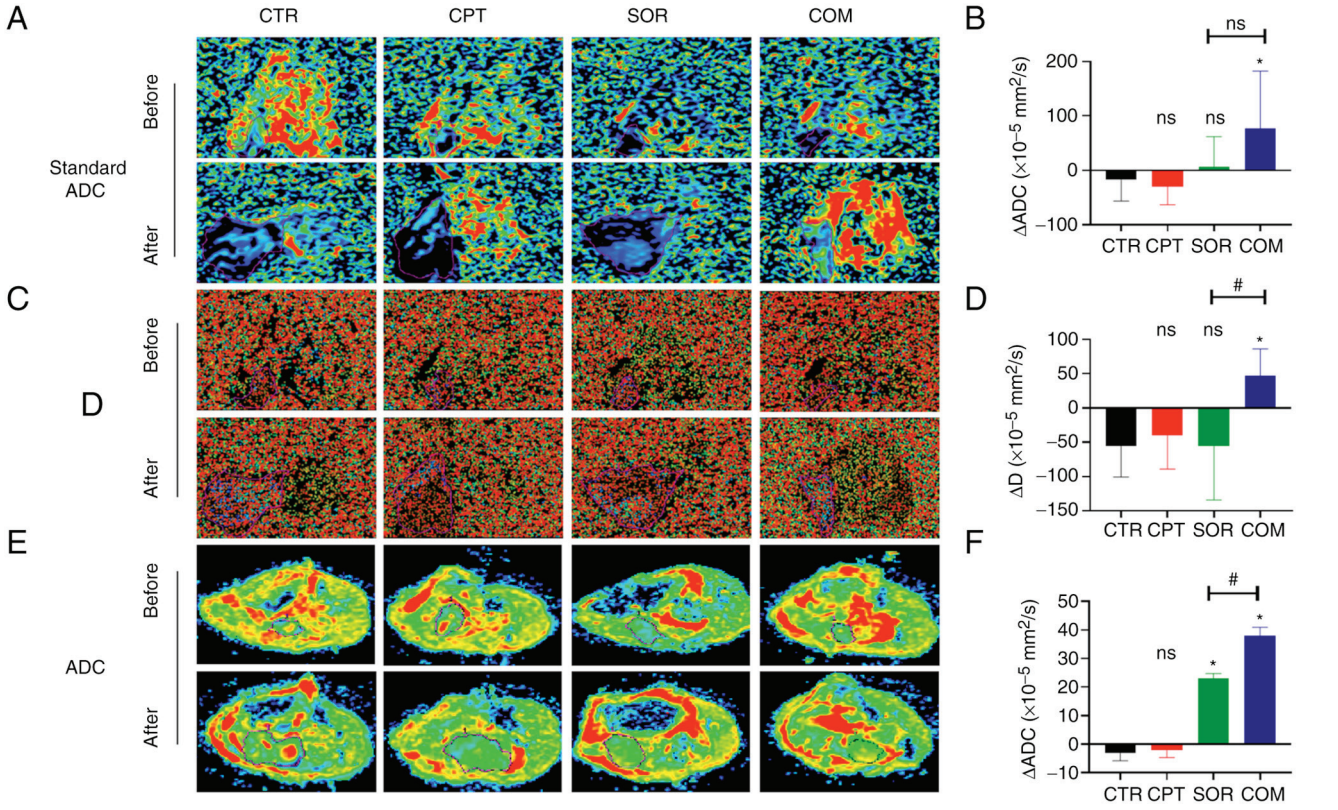

Figure 7. CPT combined with sorafenib reduces tumor activity. (A) Standard ADC values of CTR, CPT, SOR and COM groups in H22 models before and after treatment. (B) Δ standard ADC value was calculated in four groups. (C) D values of four groups in H22 models before and after treatment. (D) ΔD value was calculated in four groups. D and D* images were captured from the same samples and they differed only in the settings of the imaging parameters. (E) ADC values of four groups in VX2 models before and after treatment. (F) ΔADC value was calculated in four groups. The MRI images in panels A, C and E were enlarged according to the same scale. *P<0.05 and #P<0.05. CPT, camptothecin; Standard ADC/ADC, apparent diffusion coefficient; CTR, control; SOR, sorafenib; COM, combined; Δ Standard ADC/ADC, postoperative Standard ADC/ADC - preoperative Standard ADC/ADC; D, diffusion coefficient; ΔD, postoperative D - preoperative D; ns, no statistical significance.

than a chemotherapeutic agent. With the VX2 model, there was statistical significance between the CPT and CTR groups. The possible reason for the differences observed between the two models is that a higher CPT dose was used with the VX2 model. The expression of Nrf2 was increased in the SOR group and was inhibited in the COM group in both models, suggesting that CPT could modulate the effects of SOR on Nrf2 levels in tumor tissue. Thus, a low CPT dose could down-regulate Nrf2 levels induced by sorafenib, and its combination with sorafenib could control the growth of liver tumors. In the present study, Nrf2 and its downstream proteins, HO-1 and NQO1, were slightly higher in the CPT group than in the CTR group in the H22 model; however, these changes did not reach statistical significance. A previous study by the author showed that Nrf2 levels were low in tumor tissue without treatment, suggesting that CPT alone would not significantly inhibit or even increase Nrf2 (10). By contrast, sorafenib significantly increased Nrf2 protein in the current study. These effects were abrogated when sorafenib was combined with CPT, consistent with CPT being a modulator of Nrf2 activity.

The safety of CPT has been established, and it is used clinically as a chemotherapeutic agent (35,36). The CPT doses used in the present study (1 and 3 mg/kg) were lower than the dose used in the clinic (8 mg/kg) (10). No significant changes in weight were observed among the four treatment groups with either model and no obvious damage to the liver and kidney, indicating that the drug toxicity was within an acceptable range.

HO catalyze the decomposition of heme into carbon monoxide (CO), free iron, and biliverdin (37). HO-1 is over-expressed in HCC. CO mediates the antiapoptotic effects of HO-1, promoting tumor growth (37). Furthermore, HO-1 can regulate Nrf2-targeted ABC efflux transporters (8). NQO1 is an antioxidant related to the detoxification of quinones and the reduction of iron-mediated ROS that is upregulated by Nrf2 in response to sorafenib (6,18,20,38). NQO1 reduces sorafenib-induced ferroptosis of HCC (39). In addition, NQO1 overexpression could detoxify antitumor drugs, favoring multidrug resistance (11). The present study demonstrated that sorafenib significantly increased HO-1 and NQO1 proteins and these effects were abrogated when sorafenib was combined with CPT, consistent with Nrf2 nuclear translocation and Nrf2-ARE activation.

EMT is the biological process for tumor cell migration and invasion (26,40,41). Changing a cell phenotype from epithelial to mesenchymal is the main characteristic of EMT (40-42). The core regulators of EMT, including N-cadherin and Snail, are regulated by Nrf2 (26,40,41,43-45). N-cadherin promotes neovascularization and adhesion between tumor cells and mesenchymal cells (43). Snail regulates E-cadherin expression during EMT (43) and can also promote chemoresistance by upregulating the ABC transporter ABCB1 in HCC

cells (46). Previous studies identified EMT characteristics in sorafenib-resistant HCC cells, including the activation of the mesenchymal markers N-cadherin and Snail (46-51). A previous study revealed that EMT was inhibited after Nrf2 downregulation by CPT (26). In the current study, sorafenib + TAE treatment significantly increased N-cadherin and Snail levels in the VX2 tumors, which promotes EMT and drug resistance. The addition of CPT to the treatment decreased the EMT markers, which may be one of the reasons why CPT enhanced HCC sorafenib sensitivity (52). Moreover, fewer metastases were observed in the rabbits in COM group than in SOR group. These results are consistent with CPT-mediated Nrf2 downregulation and inhibition of EMT.

High metabolism during tumor growth leads to a hypoxic microenvironment and HIF-1α activation in tumors, which activates growth factors (e.g., VEGFA) and induces vasculature generation. Sorafenib activates HIF-1α and induces VEGFA expression, which mediates sorafenib resistance (46). Previous studies demonstrated that downregulating Nrf2 could reduce vasculature formation (53,54). In a previous study by the authors, CPT could also suppress the HIF-1α/VEGFA signaling pathway in tumors and decrease vascular quantity (26). In the current study, the levels of HIF-1α and VEGFA in the VX2 tumors from the CPT group were lower than in the CTR group, confirming that CPT could inhibit the HIF-1 α/VEGFA signaling pathway. The perfusion of tumor-feeding arteries with sorafenib and lipiodol significantly increased HIF-1α and VEGFA proteins, whereas these levels significantly decreased in the COM group. CPT also reduced VEGFA expression-induced by sorafenib in H22 model.

DWI models presume that the displacement of water molecules follows a Gaussian distribution (55). The ADC provided by these models represents an average diffusion value (55,56). However, water diffusion *in vivo* is more complex and includes water molecule diffusion and microcirculation perfusion (31,57,58). IVIM is one of the most common non-Gaussian DWI models (55). The parameters for IVIM include the Standard ADC value, representing an average diffusion value; D value that reflects the diffusion of pure water molecules, the D^* value that reflects the microcirculation perfusion, and the f value that is defined as the ratio between the perfusion of local microcirculation and diffusion overall (55). Although the differences in Δ Standard ADC and ΔD values for SOR and COM groups for the H22 model were not statistically significant, they showed an upward trend in the COM group compared with SOR group, indicating that the tumor activity of the COM group was lower than that of the SOR group. The differences between ΔD^* and Δf in SOR and COM groups were not statistically significant, either. They demonstrated a downward trend in the COM group than SOR group, reflecting that the microcirculation perfusion in the COM group was lower than in the SOR group. Similar results for ΔADC were obtained with the VX2 model. Namely, VX2 tumor activity decreased in the COM group.

In conclusion, the present study confirmed that sorafenib increased Nrf2 protein levels and promoted HCC invasion and metastasis, which may be the mechanism of sorafenib resistance. As a novel Nrf2 inhibitor, CPT combined with sorafenib significantly inhibited tumor growth and reduced tumor microcirculation perfusion and activity.

Acknowledgements

The authors would like to thank the Experimental Center of Qianfoshan Hospital of Shandong for providing relevant consultation and instrument support.

Funding

The present study was supported by the Natural Science Foundation of Shandong (grant no. ZR2019BH041), the Nature Science Foundation of China (grant no. 81803008) and the cultivating fund of the First hospital of Shandong First Medical University (grant no. QYPY2021NSFC0616).

Availability of data and materials

The datasets used and/or analyzed during the current study are available from the corresponding author on reasonable request.

Authors' contributions

FC, GL proposed ideas and completed outline. HW, FM, JZ and XL carried out the study. LS, QL and SC found the relevant literature and carried out data collection and analysis. LS wrote the original draft and edited the manuscript. FC provided final approval of the version to be published. GL supervised the study and agreed to be accountable for all aspects of the work. All authors contributed to the article and read and approved the final version of the manuscript. LS and HW confirm the authenticity of all the raw data.

Ethics approval and consent to participate

All animal experiments were performed according to the ARRIVE guidelines approved (approval no. S0007) by the Animal Care and Use Committee of the First Hospital of Shandong First Medical University (Jinan, China).

Patient consent for publication

Not applicable.

Competing interests

The authors declare that they have no competing interests.

References

1. Sung H, Ferlay J, Siegel RL, Laversanne M, Soerjomataram I, Jemal A and Bray F: Global cancer statistics 2020: GLOBOCAN estimates of incidence and mortality worldwide for 36 cancers in 185 countries. CA Cancer J Clin 71: 209-249, 2021.
2. Liu W, Quan B, Lu S, Tang B, Li M, Chen R, Ren Z and Yin X: First-line systemic treatment strategies for unresectable hepatocellular carcinoma: A systematic review and network meta-analysis of randomized clinical trials. Front Oncol 11: 771045, 2021.
3. Meyer T, Fox R, Ma YT, Ross PJ, James MW, Sturgess R, Stubbs C, Stocken DD, Wall L, Watkinson A, *et al*: Sorafenib in combination with transarterial chemoembolisation in patients with unresectable hepatocellular carcinoma (TACE 2): A randomised placebo-controlled, double-blind, phase 3 trial. Lancet Gastroenterol Hepatol 2: 565-575, 2017.

4. Sun J, Zhou C, Zhao Y, Zhang X, Chen W, Zhou Q, Hu B, Gao D, Raatz L, Wang Z, *et al*: Quiescin sulfhydryl oxidase 1 promotes sorafenib-induced ferroptosis in hepatocellular carcinoma by driving EGFR endosomal trafficking and inhibiting NRF2 activation. Redox Biol 41: 101942, 2021.
5. Zhang Y, Tan Y, Liu S, Yin H, Duan J, Fan L, Zhao X and Jiang B: Implications of Withaferin A for the metastatic potential and drug resistance in hepatocellular carcinoma cells via Nrf2-mediated EMT and ferroptosis. Toxicol Mech Methods 33: 47-55, 2022.
6. Sun X, Ou Z, Chen R, Niu X, Chen D, Kang R and Tang D: Activation of the p62-Keap1-NRF2 pathway protects against ferroptosis in hepatocellular carcinoma cells. Hepatology 63: 173-184, 2016.
7. Chen KF, Chen HL, Tai WT, Feng WC, Hsu CH, Chen PJ and Cheng AL: Activation of phosphatidylinositol 3-kinase/Akt signaling pathway mediates acquired resistance to sorafenib in hepatocellular carcinoma cells. J Pharmacol Exp Ther 337: 155-161, 2011.
8. Gao L, Morine Y, Yamada S, Saito Y, Ikemoto T, Tokuda K, Takasu C, Miyazaki K and Shimada M: Nrf2 signaling promotes cancer stemness, migration, and expression of ABC transporter genes in sorafenib-resistant hepatocellular carcinoma cells. PLoS One 16: e0256755, 2021.
9. Wang Q, Ching B, Xue Q, Gao Q, Huang A, Wang K and Tang N: GSTZ1 sensitizes hepatocellular carcinoma cells to sorafenib-induced ferroptosis via inhibition of NRF2/GPX4 axis. Cell Death Dis 12: 426, 2021.
10. Chen F, Wang H, Zhu J, Zhao R, Xue P, Zhang Q, Nelson MB, Qu W, Feng B and Pi J: Camptothecin suppresses NRF2-ARE activity and sensitises hepatocellular carcinoma cells to anticancer drugs. Br J Cancer 117: 1495-1506, 2017.
11. Tian B, Lu ZN and Guo XL: Regulation and role of nuclear factor-E2-related factor 2 (Nrf2) in multidrug resistance of hepatocellular carcinoma. Chem Biol Interact 280: 70-76, 2018.
12. Tebay LE, Robertson H, Durant ST, Vitale SR, Penning TM, Dinkova-Kostova AT and Hayes JD: Mechanisms of activation of the transcription factor Nrf2 by redox stressors, nutrient cues, and energy status and the pathways through which it attenuates degenerative disease. Free Radic Biol Med 88: 108-146, 2015.
13. Gao AM, Ke ZP, Shi F, Sun GC and Chen H: Chrysin enhances sensitivity of BEL-7402/ADM cells to doxorubicin by suppressing PI3K/Akt/Nrf2 and ERK/Nrf2 pathway. Chem Biol Interact 206: 100-108, 2013.
14. Najafi M, Mortezaee K and Majidpoor J: Cancer stem cell (CSC) resistance drivers. Life Sci 234: 116781, 2019.
15. Shibue T and Weinberg RA: EMT, CSCs, and drug resistance: The mechanistic link and clinical implications. Nat Rev Clin Oncol 14: 611-629, 2017.
16. Huang T, Song X, Xu D, Tiek D, Goenka A, Wu B, Sastry N, Hu B and Cheng SY: Stem cell programs in cancer initiation, progression, and therapy resistance. Theranostics 10: 8721-8743, 2020.
17. Niture SK, Khatri R and Jaiswal AK: Regulation of Nrf2-an update. Free Radic Biol Med 66: 36-44, 2014.
18. He F, Ru X and Wen T: NRF2, a transcription factor for stress response and beyond. Int J Mol Sci 21: 4777, 2020.
19. He F, Antonucci L and Karin M: NRF2 as a regulator of cell metabolism and inflammation in cancer. Carcinogenesis 41: 405-416, 2020.
20. Tonelli C, Chio IIC and Tuveson DA: Transcriptional regulation by Nrf2. Antioxid Redox Signal 29: 1727-1745, 2018.
21. Zhang DD, Lo SC, Cross JV, Templeton DJ and Hannink M: Keap1 is a redox-regulated substrate adaptor protein for a Cul3-dependent ubiquitin ligase complex. Mol Cell Biol 24: 10941-10953, 2004.
22. Hayes JD McMahon M, Chowdhry S and Dinkova-Kostova AT: Cancer chemoprevention mechanisms mediated through the Keap1-Nrf2 pathway. Antioxid Redox Signal 13: 1713-1748, 2010.
23. Gao L, Morine Y, Yamada S, Saito Y, Ikemoto T, Tokuda K, Miyazaki K, Okikawa S, Takasu C and Shimada M: The BAFF/NFκB axis is crucial to interactions between sorafenib-resistant HCC cells and cancer-associated fibroblasts. Cancer Sci 112: 3545-3554, 2021.
24. Lu MC, Ji JA, Jiang ZY and You QD: The Keap1-Nrf2-ARE pathway as a potential preventive and therapeutic target: An update. Med Res Rev 36: 924-963, 2016.
25. Robertson H, Dinkova-Kostova AT and Hayes JD: NRF2 and the ambiguous consequences of its activation during initiation and the subsequent stages of tumourigenesis. Cancers (Basel) 12: 3609, 2020.
26. Liu Q, Zhao S, Meng F, Wang H, Sun L, Li G, Gao F and Chen F: Nrf2 down-regulation by camptothecin favors inhibiting invasion, metastasis and angiogenesis in hepatocellular carcinoma. Front Oncol 11: 661157, 2021.
27. Kitamura H and Motohashi H: NRF2 addiction in cancer cells. Cancer Sci 109: 900-911, 2018.
28. Tang XJ, Han M, Yang B, Shen YQ, He ZG, Xu DH and Gao JQ: Nanocarrier improves the bioavailability, stability and antitumor activity of camptothecin. Int J Pharm 477: 536-545, 2014.
29. Tang W, Chen Z, Zhang W, Cheng Y, Zhang B, Wu F, Wang Q, Wang S, Rong D, Reiter FP, *et al*: The mechanisms of sorafenib resistance in hepatocellular carcinoma: Theoretical basis and therapeutic aspects. Signal Transduct Target Ther 5: 87, 2020.
30. Zheng A, Chevalier N, Calderoni M, Dubuis G, Dormond O, Ziros PG, Sykiotis GP and Widmann C: CRISPR/Cas9 genome-wide screening identifies KEAP1 as a sorafenib, lenvatinib, and regorafenib sensitivity gene in hepatocellular carcinoma. Oncotarget 10: 7058-7070, 2019.
31. Tang X, Wang H, Fan L, Wu X, Xin A, Ren H and Wang XJ: Luteolin inhibits Nrf2 leading to negative regulation of the Nrf2/ARE pathway and sensitization of human lung carcinoma A549 cells to therapeutic drugs. Free Radic Biol Med 50: 1599-1609, 2011.
32. Murakami Y, Sugiyama K, Ebinuma H, Nakamoto N, Ojiro K, Chu PS, Taniki N, Saito Y, Teratani T, Koda Y, *et al*: Dual effects of the Nrf2 inhibitor for inhibition of hepatitis C virus and hepatic cancer cells. BMC Cancer 18: 680, 2018.
33. Arlt A, Sebens S, Krebs S, Geismann C, Grossmann M, Kruse ML, SchreiberS and Schäfer H: Inhibition of the Nrf2 transcription factor by the alkaloid trigonelline renders pancreatic cancer cells more susceptible to apoptosis through decreased proteasomal gene expression and proteasome activity. Oncogene 32: 4825-4835, 2013.
34. Wang XJ, Hayes JD, Henderson CJ and Wolf CR: Identification of retinoic acid as an inhibitor of transcription factor Nrf2 through activation of retinoic acid receptor alpha. Proc Natl Acad Sci U S A 104: 19589-19594, 2007.
35. Bailly C: Irinotecan: 25 years of cancer treatment. Pharmacol Res 148: 104398, 2019.
36. de Lucas Chazin E, da Rocha Reis R, Junior WT, Moor LF and Vasconcelos TR: An overview on the development of new potentially active camptothecin analogs against cancer. Mini Rev Med Chem 14: 953-962, 2014.
37. Sass G, Barikbin R and Tiegs G: The multiple functions of heme oxygenase-1 in the liver. Z Gastroenterol 50: 34-40, 2012.
38. Leung HW, Lau EYT, Leung CON, Lei MML, Mok EHK, Ma VWS, Cho WCS, Ng IOL, Yun JP, Cai SH, *et al*: NRF2/SHH signaling cascade promotes tumor-initiating cell lineage and drug resistance in hepatocellular carcinoma. Cancer Lett 476: 48-56, 2020.
39. Dai C, Chen X, Li J, Comish P, Kang R and Tang D: Transcription factors in ferroptotic cell death. Cancer Gene Ther 27: 645-656, 2020.
40. Zhang G and Zhang G: Upregulation of FoxP4 in HCC promotes migration and invasion through regulation of EMT. Oncol Lett 17: 3944-3951, 2019.
41. Wang Y, Shi J, Chai K, Ying X and Zhou BP: The role of snail in EMT and tumorigenesis. Curr Cancer Drug Targets 13: 963-972, 2013.
42. Giannelli G, Koudelkova P, Dituri F and Mikulits W: Role of epithelial to mesenchymal transition in hepatocellular carcinoma. J Hepatol 65: 798-808, 2016.
43. Gheldof A and Berx G: Cadherins and epithelial-to-mesenchymal transition. Prog Mol Biol Transl Sci 116: 317-336, 2013.
44. Al Khatib AM, Mărgăritescu C, Taisescu O, Andreiana BC, Florescu MM and Ciurea RN: Immunoexpression of E-cadherin, snail and twist in colonic adenocarcinomas. Rom J Morphol Embryol 60: 531-536, 2019.
45. Tian Y, Qi P, Niu Q and Hu X: Combined snail and E-cadherin predicts overall survival of cervical carcinoma patients: Comparison among various epithelial-mesenchymal transition proteins. Front Mol Biosci 7: 22, 2020.
46. Zhao H, Cheng X, Yu J and Li Y: Stabilization of snail maintains the sorafenib resistance of hepatocellular carcinoma cells. Arch Biochem Biophys 699: 108754, 2021.
47. Chen HA, Kuo TC, Tseng CF, Ma JT, Yang ST, Yen CJ, Yang CY, Sung SY and Su JL: Angiopoietin-like protein 1 antagonizes MET receptor activity to repress sorafenib resistance and cancer stemness in hepatocellular carcinoma. Hepatology 64: 1637-1651, 2016.

48. van Malenstein H, Dekervel J, Verslype C, Van Cutsem E, Windmolders P, Nevens F and van Pelt J: Long-term exposure to sorafenib of liver cancer cells induces resistance with epithelial-to-mesenchymal transition, increased invasion and risk of rebound growth. Cancer Lett 329: 74-83, 2013.
49. Zhao CX, Luo CL and Wu XH: Hypoxia promotes 786-O cells invasiveness and resistance to sorafenib via HIF-2α/COX-2. Med Oncol 32: 419, 2014.
50. Liu H, Wang M, Liang N and Guan L: PDCD2 sensitizes HepG2 cells to sorafenib by suppressing epithelialmesenchymal transition. Mol Med Rep 19: 2173-2179, 2019.
51. Chen W, Yang J, Zhang Y, Cai H, Chen X and Sun D: Regorafenib reverses HGF-induced sorafenib resistance by inhibiting epithelial-mesenchymal transition in hepatocellular carcinoma. FEBS Open Bio 9: 335-347, 2019.
52. Mir N, Jayachandran A, Dhungel B, Shrestha R and Steel JC: Epithelial-to-mesenchymal transition: A mediator of sorafenib resistance in advanced hepatocellular carcinoma. Curr Cancer Drug Targets 17: 698-706, 2017.
53. Ji X, Wang H, Zhu J, Zhu L, Pan H, Li W, Zhou Y, Cong Z, Yan F and Chen S: Knockdown of Nrf2 suppresses glioblastoma angiogenesis by inhibiting hypoxia-induced activation of HIF-1α. Int J Cancer 135: 574-584, 2014.
54. Kim TH, Hur EG, Kang SJ, Kim JA, Thapa D, Lee YM, Ku SK, Jung Y and Kwak MK: NRF2 blockade suppresses colon tumor angiogenesis by inhibiting hypoxia-induced activation of HIF-1α. Cancer Res 71: 2260-2275, 2011.
55. Tramontano L, Cavaliere C, Salvatore M and Brancato V: The role of non-gaussian models of diffusion weighted MRI in hepatocellular carcinoma: A systematic review. J Clin Med 10: 2641, 2021.
56. Zhou Y, Yang G, Gong XQ, Tao YY, Wang R, Zheng J, Yang C, Peng J, Yang L, Li JD and Zhang XM: A study of the correlations between IVIM-DWI parameters and the histologic differentiation of hepatocellular carcinoma. Sci Rep 11: 10392, 2021.
57. Le Bihan D, Breton E, Lallemand D, Grenier P, Cabanis E and Laval-Jeantet M: MR imaging of intravoxel incoherent motions: Application to diffusion and perfusion in neurologic disorders. Radiology 161: 401-407, 1986.
58. Granata V, Fusco R, Filice S, Catalano O, Piccirillo M, Palaia R, Izzo F and Petrillo A: The current role and future prospectives of functional parameters by diffusion weighted imaging in the assessment of histologic grade of HCC. Infect Agent Cancer 13: 23, 2018.